Hydrogeology Journal
https://doi.org/10.1007/s10040-024-02822-x

REPORT

Contribution of the time domain electromagnetic method to the study of the Kalahari transboundary multilayered aquifer systems in Southern Angola

Alain P. Francés[1] · Elsa C. Ramalho[1] · Fernando Monteiro Santos[2] · José M. Llorente[3] · Teodora Mateus[4,5] · Raquel Martín-Banda[3] · Ivan Cuervo[4] · José Luis García Lobón[3] · Valter Dala[6] · Manuel Ditutala[6] · Abreu Famorosa[6] · Américo da Mata Victorino[6,7]

Received: 1 November 2023 / Accepted: 2 August 2024

Abstract

The Cunene Province (Southern Angola) is facing recurrent and pluriannual droughts. Surface water supply could be reinforced using the groundwater resources of the multilayered aquifer systems (MAS) hosted in the siliciclastic sediments of the Kalahari Group. The MAS were first identified in the early 2000s in Northern Namibia and recently in the Cunene Province, by studies of the PLANAGEO project based on modern processing and reinterpretation of legacy data from the 1960s and 1970s (electrical resistivity data and deep boreholes). This article presents the results of a time domain electromagnetic (TDEM) survey conducted in the Cunene Province to: (i) contribute to the design of the hydrogeological conceptual model of the transboundary MAS, namely their geometry and extension; (ii) validate the reprocessing of the legacy data; and (iii) guide the future location of boreholes. Results depict the geometry of the sedimentary basin and the characterization of the MAS, with particular emphasis on the intermediate and deep aquifers. The borehole siting, based on the interpretation of the new TDEM data and the legacy data (clay markers in borehole logs), was successful, with a good agreement between estimated and observed horizons of the deep aquifers. However, the presence of clayey layers, a clay-rich matrix in the detrital deposits and saline/brackish groundwater led to uncertainties in the interpretation of the electrical transects. As such, recommendations are made to improve future data collection and mapping of the MAS.

Keywords Angola · Cunene Province · Transboundary multilayered aquifer systems · Geophysical methods · Time domain electromagnetics

✉ Alain P. Francés
alain.frances@lneg.pt

1 National Laboratory of Energy and Geology (LNEG), Estrada da Portela, Bairro Do Zambujal, Apartado 7586, 2610-999 Amadora, Alfragide, Portugal

2 Faculty of Sciences of the University of Lisbon – Institute D. Luiz, Campo Grande C8, 1749-016 Lisbon, Portugal

3 Geological and Mining Institute of Spain, Spanish National Research Council (IGME-CSIC), C/ La Calera, 1, 28760 Madrid, Tres Cantos, Spain

4 Temporary Union of Companies (UTE) - Impulso Angola, Rua Ndunduma 85, Miramar, Luanda, Angola

5 Cuvelai Watercourse Commission (CUVECOM), GABHIC, Caculuvale, Ondjiva, Cunene, Angola

6 Geological Institute of Angola (IGEO), Rua 311, Centralidade Do Kilamba, Belas, Luanda, Angola

7 Faculty of Natural Sciences of the University Agostinho Neto, Av. 4 de Fevereiro, 71, Luanda, Angola

Introduction

The Cunene Province (ca. 87 000 km^2), located in Southern Angola, is characterized by an arid and hot climate, with low and irregular rainfall and high potential evapotranspiration (Feria et al. 2021; Serrat-Capdevila et al. 2022). These climatic characteristics lead to recurrent and pluriannual droughts that dramatically affect the population, by limiting the water supply available to livestock rearing and other agricultural activities. This situation not only drastically limits economic development but also causes frequent humanitarian crises, as ca. 800,000 people of the total population of ca. 990,000 inhabitants are scarcely dispersed throughout the province, living in small family units and farms, called *quimbos* (INE 2016). Traditionally, water supply was satisfied by the Cunene River or through *chimpacas* (large shallow

Published online: 17 September 2024

ponds that collect rainwater and runoff coming from small catchments) and *cacimbas* (hand-dug wells 4–5 m deep, excavated in riverbeds or other loose sediments). However, with the increase in frequency and duration of droughts, access to surface water is no longer reliable and so groundwater potential should be further explored, especially the presence of deep groundwater resources (Serrat-Capdevila et al. 2022).

In Southern Angola and Northern Namibia, the Owambo Basin (Miller et al. 2010) hosts transboundary, multilayered aquifer systems that are currently under characterization. In the decade of 2000, the Kalahari-Ohangwena (KOH) and the Kalahari-Oshana (KOS) aquifer systems were identified (Margane et al. 2005; Schildknecht 2012). However, while the KOS lacks sedimentary, stratigraphic and hydrogeological information either in Angola or in Namibia, the KOH was subject to extensive studies in the Northern Namibian sector of the Cuvelai-Etosha Basin (Dill et al. 2013; Himmelsbach et al. 2018; Houben et al. 2020; Lindenmaier and Christelis 2011; Lindenmaier et al. 2012, 2014; Schildknecht 2012; Wallner et al. 2017). These authors carried out extensive time domain electromagnetic (TDEM) surveys along transects (ca. 50–300 km long) transversal and longitudinal to the Cubango Megafan, drilling campaigns with cutting and core sampling, geophysical borehole logs, pumping tests and hydrochemical, isotopic and clay mineral analysis to define the hydrostratigraphy of the KOH. These authors identified and characterized a deep aquifer that contains fresh water in some zones that may have an important role in water supply.

In Angola, during the decades of 1960–1970, the project "Plano de Coordenação para o Abastecimento de Água às Regiões Pastorícias do Sul de Angola – PCAARPSA" (Coordination Plan for Water Supply to Pastoral Regions of Southern Angola, 1966 in Gomes (1972)) was launched and developed to evaluate the groundwater potential of the Kalahari sediments deeper than 100 m with the aim of providing water supply to population and livestock (Gomes 1972; Motta Marques 1967; Neves Ferrão 1961; Neves Ferrão 1966; Pacheco 1976). These works were interrupted for more than 40 years, due to the colonial and civil wars. Recently, studies based on modern processing and reinterpretation of legacy data (Ramalho et al. 2023b), validated with boreholes (Gomes 1972) and TDEM (Schildknecht 2012) data, pointed out the extension of the KOS and KOH in the Cunene Province, in Southern Angola. The present work intends to confirm this hypothesis by conducting a TDEM survey, within the framework of the "Plano Nacional de Geologia" (PLANAGEO) project, that will contribute to the definition of the conceptual model of the transboundary aquifer systems, namely their geometry and extension.

Materials and methods

Geomorphology and hydrology

The hydrological Cuvelai-Etosha basin (CEB) forms a large endorheic basin that extends from the base of the Angolan Highlands towards north-central Namibia (Fig. 1). Between the Cunene and the Cubango Rivers, the landscape is characterized by a flat terrain of arenosols covered by open woodland composed of sparsely distributed trees, typical of savannah environments. The topography is gentle and monotonous, with a very small topographical gradient towards south (the slope gradient in the N-S direction of Fig. 1 is ca. 0.04%). The terrain is cut by ephemeral and paleodrainage channels, which are dry most of the time. In the center of the province lies the Chana drainage area, characterized by a dense network of channels, showing an alternance of *chanas* and *ecangos*, which correspond to paleostreams with clayey soil, separated by *mufitos*, which are slightly elevated zones covered by a bushy vegetation and grass (Feio 1966; Mendelsohn and Mendelsohn 2018). This micromorphology results from the dynamic of the paleo-Cunene fluvial system, which was flowing towards the Etosha Lake in an endoreic basin. The capture of the Cunene River towards the Atlantic Ocean, 4 My ago during the Pliocene (Feio 1966, 1970; Gumiel et al. 2018; Miller et al. 2010), deactivated the paleo-Cunene fluvial system. Since then, *chanas* and *ecangos* are only fed by direct rainfall and by the modern Cuvelai drainage system, acting as surface water reservoirs that are widely used for human and livestock water supply and fishing.

Geology

The CEB is contained by the Owambo Basin, which is bounded to the north and west by the Precambrian rocks of the Angolan Highlands, and in the South by the Damara Belt and in the east by the Cubango River. The Owambo Basin formed during the Late Proterozoic distension related to the fragmentation of the Rodinia supercontinent (Miller et al. 2010). On top of the sediments of the Damara Sequence and Karoo Supergroups, the CEB accommodates ca. 600 m thick succession of siliciclastic sediments of the Kalahari Group, from the Upper Cretaceous to Pliocene (Miller et al. 2010). In Namibia, the following units were recognized, from the base to the top (Houben et al. 2020; Lindenmaier et al. 2014): the red Ombalantu Formation, the conglomeratic Beiseb Formation, the Olukonda Formation and the white Andoni Formation. The Olukonda Formation (Paleocene-late Eocene) is composed of

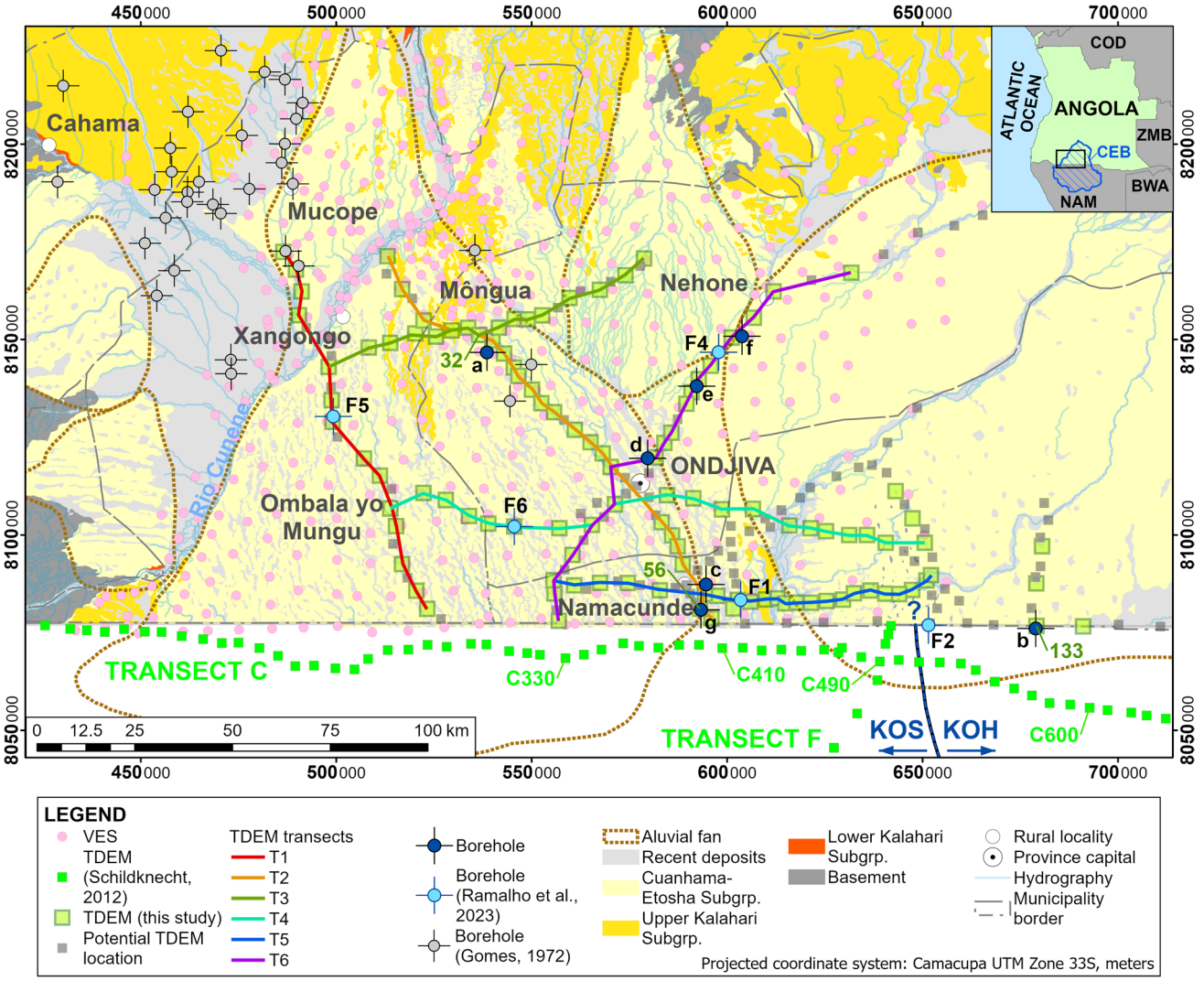

Fig. 1 Geological sketch map of Cunene Province with the location of the TDEM soundings and associated transects that were used for quasi-2D inverse modelling. The boreholes F1 to F6 were drilled in the framework of the project PLANAGEO (Ramalho et al. 2023a) and the vertical electrical soundings (VES) of Ramalho et al. (2023b) are also represented. The dark green labels (32, 56 and 133) correspond to the ID of the TDEM referred to in Fig. 4. The light green labels (C330, C410, C490, C600, Transects C and F) correspond to the ID of the TDEM of Schildknecht (2012) referred in Fig. 7. a: PS-1 Mongua (Gomes 1972); b: 101,047 (Lindenmaier et al. 2014); c: Namacunde (Gomes 1972); d: Mucuíula (Gomes 1972); e: Nonapa (Gomes 1972); f: Noema (Gomes 1972); g: CFRL-2 (CFRL, Angola). KOH: Kalahari-Ohangwena aquifer systems. KOS: Kalahari-Oshana aquifer systems. CEB: Cuvelai-Etosha Basin. COD: Democratic Republic of the Congo. BWA: Botswana. ZMD: Zambia

a succession of red-bed sands with layers on the meter scale, consolidated and semi-consolidated with white calcretes and dolocretes, with intercalations of clays. The sediments originate from the weathering of the Cunene Intrusive Complex, in Angola, and were transported and deposited by the paleo-Cunene River, flowing southeast and east, forming a large fluvial fan 360 km long, 260 km wide and 275–400 m thick, between the Paleoecene and late Eocene (Gärtner et al. 2023; Houben et al. 2020). A new erosion–deposition cycle led to the deposition of the Andoni Formation during the Late Eocene-Pliocene (Labaredas and Oliveira 2021a). This unit is characterized by white fine sands, clayey sands and clay with some intercalations of limestones and calcretes (Houben et al. 2020; Lindenmaier et al. 2014). It is associated with the Cubango Megafan, which transported, between the Eocene and the Pliocene, sediments originating from the Paleoproterozoic to Damaran/Pan-African felsic metamorphic and granitoid rocks from the Angolan Highlands, located to the N and NE, up to the NE of the Etosha Pan (Gärtner et al. 2023; Houben et al. 2020). The base of the Andoni Formation is composed of red sandy silts and clayey silts that mark the

transition with the underlying Olukonda Formation (Houben et al. 2020). These latter authors associated the upper part of the Olukonda Formation, as defined by Lindenmaier et al. (2014), to the base of the Andoni Formation. They justified such statement by hypothesizing that the Cunene River deviated towards the Ocean Atlantic during the Eocene and that a Cunene Megafan concomitant of the Cubango Megafan (Lindenmaier et al. 2014; Miller et al. 2010) did not exist. Instead, the deposits in the western part of the Owambo Basin correspond to an overbank fan of the Cunene River, more clayey than the sediments of the Cubango Megafan. On the other hand, the distal western facies of the Cubango Megafan are also characterized by a dominant clay content. These two hypotheses have important hydrogeological consequences, as discussed in the next section.

In Southern Angola, the geology of the northern part of the Owambo Basin (Fig. 1), as well as its transition towards the main planation surface of central Angola (Planalto Principal, sensu Feio 1981), was established some decades ago (e.g. Carvalho et al. 1973a, 1973b, Carvalho 1982; Pacheco 1976) and was recently completed within the framework of the PLANAGEO project, which aimed to cover Angola with continuous and complete geological cartography (Escuder-Viruete et al. 2018; Feria et al. 2021; Gumiel et al. 2018; Labaredas and Oliveira 2021a, b, c; Martín-Banda et al. 2020; Oliveira and Sousa 2021; Sousa et al. 2021a, b). In Angola, the full sequence of the Cenozoic intracratonic deposits are outcropping, which facilitated the analysis and the definition of the litostratigraphic units of the Kalahari Group, although its lower part is only exposed in small areas generally in valleys. Moreover, the transition towards the plateau allows relating the internal sequences with the pediplanation surfaces which give insights to elaborate a model of the morphotectonic and sedimentary evolution of the region (Rodrigues and Marques 2021). On other hand, in Namibia the sequence was characterized through the analysis of deep borehole cores, as only the top of the sequence is outcropping (Miller 1992; Houben et al. 2020).

The Lower Kalahari Subgroup (Eocene–Oligocene) is the basal unit that was deposited on the African surface, i.e. the early Cenozoic regional peneplanation surface that is well preserved in several places across Southern-Africa (Labaredas and Oliveira 2021a). It is composed by silcretized and calcretized sandstones, conglomerates, limestones and red clays, and are well-known in Angola under the designation "Grés Polimorfos" Formation. Its equivalent defined in the Namibian sector of the Owambo Basin is the Olukonda Formation (Labaredas and Oliveira 2021a). The top of this unit is characterized by a hardpan made of ferricrete and ferritic conglomerates that is overlaid by the Upper Kalahari Subgroup (Miocene-Pliocene), composed by ca. 100 m of unconsolidated sands, known in Angola as "Areias Ocres" Formation. The Lower Kalahari Subgroup outcrops sparsely in the north of the Cunene Province along the incised valley of the main streams, whereas the Upper Kalahari Subgroup is more widespread in this region (Fig. 1). This latter unit was overlain by prograding sandy and clayey layers, also characterized by the presence of calcretes (hardpans and nodules), of the Cubango, Cunene and Cuvelai fluviodeltaic paleosystems. These paleosystems formed the deposits of the Cuanhama-Etosha Subgroup (Pliocene–Pleistocene), which occupy most of the area of the Cunene Province (Fig. 1). The equivalent unit of this Subgroup in Namibia is the Andoni Formation. Around 4 Ma, an extreme arid event promoted the drying of the Etosha Lake and the fluvial system was replaced by an eolian system that gave origin to the paleodunes deposits of the N'Guanguela Formation, from the Late Pleistocene-Holocene, which partially overlie the Kalahari Group. They correspond to beige and sometimes red unconsolidated fine to medium eolian sands. Finally, around 1 Ma, a more humid climate promoted the development of the present hydrographic network, largely due to the deviation of the Cubango River towards the Okavango Delta in the southeast and the deepening of the Cunene River Valley (Houben et al. 2020).

Hydrogeology

A key hydrogeological characteristic of the multilayered aquifer systems of the Owambo Basin is their pronounced heterogeneity, due to the fluvio-deltaic origin of the geological units. The alternation of hydrogeologically favorable sandy layers with unfavorable clays and duricrusts (Haddon 2005), frequent lateral facies changes and the lack of outcrops provide challenges to groundwater exploration and therefore reduce the success rate of productive boreholes (Christelis and Struckmeier 2011). Moreover, groundwater from most of the aquifers feature high salinities that prohibits their use for livestock and human consumption and even for crop irrigation.

Groundwater exploration in Southern Angola throughout the decades of 1960–70 (Gomes 1972; Motta Marques 1967; Neves Ferrão 1961, 1966; Pacheco 1976) comprised: (i) an extensive geoelectrical survey with 482 vertical electrical soundings (VES) using the Schlumberger array with maximum current electrode spacings varying between 700 and 2400 m, carried out in the Cunene Province with the aim of resolving the thickness of the sedimentary basin (Nascimento and Farinha 1967; Nascimento et al. 1966, 1967); and (ii) a drilling survey of 37 deep (> 100 m) boreholes (Gomes 1972) in the region west of Ondjiva up to North of Xangongo (Fig. 1). These legacy datasets were recently reprocessed and reinterpreted to create a 3D geoelectrical model for the Cunene area (Ramalho et al. 2023b). The establishment of a connection with the aquifer systems recognized

in Northern Namibia (Lindenmaier et al. 2014; Margane et al. 2005; Schildknecht 2012) is ongoing, using the 3D geoelectrical model together with the new geological survey carried out within the framework of the PLANAGEO project (Escuder-Viruete et al. 2018; Feria et al. 2021; Gumiel et al. 2018; Labaredas and Oliveira 2021a; Martín-Banda et al. 2020), the present work and the drilling of five boreholes with geophysical logging (Ramalho et al. 2023a).

Since the early 2000, Northern Namibia has been intensively investigated to prospect and map the aquifer systems (Christelis and Struckmeier 2011; Bittner Water Consult 2006; Lindenmaier and Christelis 2011; Lindenmaier et al. 2012; Margane et al. 2005; Schildknecht 2012). These studies identified the Olukonda and Andoni Formation as hosts of multilayered aquifer systems with hydrogeological and hydrochemical characteristics that differ either in productivity or quality (Houben et al. 2020; Lindenmaier et al. 2014; Margane et al. 2005; Schildknecht 2012). Two separate aquifer systems that have extension in Angola, in the Cunene Province, were recognized: (i) the Kalahari-Ohangwena (KOH, hosted in the deposits of the Cubango Megafan); and (ii) the Kalahari-Oshana (KOS, hosted in the deposits of the Cunene River). The KOH is composed of three main aquifers (Lindenmaier et al. 2014): (i) the shallow aquifer (KOH-0), which supports perched aquifers (< 40 m) with local interest for water supply of *quimbos*; (ii) the intermediate, continuous aquifer (KOH-1), located at depth between 60 and 120 m and characterized by high salinity; (iii) the deep (> 200 m), semi-fossil aquifer (KOH-2), which has shown to have extensive and continuous layers of drinking water and thus presents a regional interest for groundwater supply. The aquifers of the KOH are separated by clayey aquitards. While the KOH-0 and the KOH-1 are hosted in the Andoni Formation, the KOH-2 is hosted in the Olukonda Formation (Lindenmaier et al. 2014). However, recently, Houben et al. (2020), complemented by Gärtner et al. (2023), analyzed a 400 m long cored borehole and found evidence that the KOH-2 is hosted in the base of the Andoni Formation. These authors stated that the Olukonda Formation, which corresponds to the Cunene Megafan with sediment source in the Cunene Mafic Complex, has poor aquifer properties due to its thin, calcrete-cemented layers and the presence of interbedding expansive clay beds. The overlying deposits, concomitant with the Andoni Formation, would correspond to the overbank fan of the Cunene River, deposited during major flooding events. Moreover, clayey units found in the area of the cored borehole would correspond to the distal western facies of the Cubango Megafan. The limit between the deposits of the overbank fan of the Cunene River and the distal facies of the Cubango Megafan is nowadays undefined. Indeed, the KOS aquifer system is lacking information and studies and, so far, only a shallow aquifer, the KOS-0, hosted in the upper 80 m of the Andoni Formation, was identified (Schildknecht 2012). The 3D geoelectrical model of the 1966–67 survey does not clearly mark the boundaries of both KOH and KOS aquifer systems (Ramalho et al. 2023b). In Angola, the drilling campaign reported by Gomes (1972), mainly carried out in the region of Mucope (NW of Xangongo, see Fig. 1), indicated very low to inexistent groundwater potential, based on low productivity or high salinity of productive boreholes. In the Mucope region, a regional, saline aquifer was detected between 70 and 100 m, characterized by the presence of palygorskite, sepiolite and zeolite clinoptilolite (Gomes 1972). This author verified the same characteristics in the boreholes drilled on the South bank of the Cunene River, with a deepening of the aquifers towards the southeast. Moreover, the top of the "Grés polimorfos" Formation (Lower Kalahari Subgroup) was associated with the presence of palygorskite and sepiolite (Plg/Sep). These minerals, associated with magnesium carbonates, would have been formed by chemical precipitation in depressions, equivalent to the actual *ecangos*, spread on the erosion surface separating the Lower and the Upper Kalahari/Cuanhama-Etosha Subgroups. As such, the thickness of this aquifer is quite variable, depending not only on the paleotopography and the depth of the depressions but also on vertical movements of local blocks due to regional tectonic framework. The clinoptilolite occurs in fine to medium sands, with low clay content and calcite carbonate cement, and is stratigraphically located above the one characterized by the presence of Plg/Sep. These clay minerals are relevant as they constitute stratigraphic and hydrogeological markers, being of assistance to map the extension and continuity of aquifers at the basin scale.

Hydrogeophysics

The geological units of the basin are characterized by a significant proportion of clay and the presence of brackish and saline groundwater, which lead to low to very low electrical resistivity of the bulk formations. Since both situations occur either in the KOH or the KOS, a more accurate analysis comprising both the 3D geoelectrical model based on legacy data (Ramalho et al. 2023b) and present-to-day data was required. Considering the hydrogeological environments that could be found in the area, Schildknecht (2012) and Lindenmaier et al. (2014) attributed the three electrical resistivity ranges presented in Table 1, while in this paper four ranges were used based on the results of reprocessed VES data (Ramalho et al. 2023b).

Data acquisition

The TDEM method was selected due to its sensitivity to high electrical conductivity, its high-speed acquisition rate and

Table 1 Ranges of electrical resistivities of the hydrogeological domains

Hydrogeological domains	Electrical resistivity range (ohm.m)	
	Schildknecht (2012) Lindenmaier et al. (2014)	Ramalho et al. (2023b) and this paper
Sands containing saline water or clay sediment	0–3	0–5
Sands containing brackish water	3–20	5–20
Sands containing freshwater	> 20	20–100
Basement	Not defined	> 100

the inexistence of ambient noise in most of the study area. Moreover, this method can reach depths of the same order of magnitude as the depth of the KOH deep aquifer (up to ca. 400 m). Data acquisition was therefore conducted with an ABEM WalkTEM 2 device, with a TX-60 transmitter connected to a square 200 × 200 m loop and a RX receiver connected to a RC-200 antenna with a square shape of 10 m side and two turns (Fig. S1 of the electronic supplementary material (ESM)). Electrical power was provided by eight 12V batteries of 75 A/h, reaching an electric current of 96 A.

The design of the acquisition scheme was implemented to fulfil the following requirements: (i) to cover the whole study area; (ii) to give insights on the longitudinal and lateral hydrostratigraphy of the basin; (iii) to be logistically feasible, in a time-limited survey with difficult conditions constraining the loop location (mostly related to accessibility and the possible existence of land and tank mines); (iv) to be possible to correlate with the previous geophysical and hydrogeological surveys carried out in the Cunene province and in Namibia. Their precise location was made over high-resolution satellite photos (Google services, ESRI, Bing) to select *quimbos* and ploughed fields to minimize the risks of land or tank mines. Moreover, a previous demining survey was made prior to each loop before its field setup and data acquisition.

The survey was carried out between 28/05/2021 and 15/07/2021 (38 days of data acquisition for a journey of 48 days), at the beginning of the dry season. The field data acquisition rate was remarkably high under such adverse conditions (long daily travelling on sandy, dirt roads), with an average of three loops/day (ca. two hours for each site). From the 197 potential locations, TDEM data (soundings) were acquired in 112 locations (Fig. 1) due to the above-mentioned constraints. The selection of the survey sites was based on the results of the previously conducted TDEM surveys and on the groundwater potential of some areas, which was indicated by previous studies. The loops were located 2–4 km apart from each other and distributed along 6 transects (Fig. 1) that were transversal (transects T1 and T2) and longitudinal (T3 to T6) to the basin. Data quality was very good due to the lack of anthropic electromagnetic fields in the area, except near the urban areas (Xangongo and Ondjiva), where data acquisition was not possible (high level of electromagnetic noise).

1D and quasi-2D data processing

The 1D inversion of the TDEM data was conducted using SPIA (Aarhus Geosoftware 2022, based on Auken et al. 2005; Auken et al. 2009; Foged et al. 2013; Kirkegaard and Auken 2014), following the workflow presented in Fig. 2. Both smooth and layered inversions are available within the software. The smooth inversion presents a large number of layers (9–30 layers) with fixed thicknesses, while vertical constraints are applied on the resistivity of adjacent layers. The layered inversion uses a few layers with no constraint on thickness and resistivity. First the data were inverted with the smooth method, using default parameters, to ensure that the data yielded reasonable and interpretable results, as well as to check the consistency with adjacent TDEM soundings. Next, a layered inversion was performed using starting models based on the information of the borehole data of Gomes (1972), other boreholes with lithological logs or other valuable information such as well-logging and local expert knowledge of the regional and local hydrogeology. The results of the 1D layered inversion were subsequently used for the hydrogeophysical interpretation, as it provided a more satisfactory representation of the regional hydrostratigraphy relative to the smooth inversion.

Data residual (DR) for the inversion model results is computed in the SPIA software, both for smooth and layered inversions, as following:

$$\mathrm{DR} = \sqrt{\frac{1}{n} \bullet \sum_{i=1}^{n} \frac{\left(d_{\mathrm{obs},i} - d_{\mathrm{sim},i}\right)^2}{\left(\sigma_i \cdot d_{\mathrm{obs},i}\right)}} \quad (1)$$

where d_{obs} is the measured value, d_{sim} is the simulated value, σ is the data uncertainty stated as a standard deviation e.g. 0.05 (i.e. 5% uncertainty), and n is the number of data points. A DR of 1 corresponds to a fit to the data standard deviation for the sounding, while a residual below 1 means that the model fits the data within the standard deviation (Aarhus Geosoftware 2022).

Quasi-2D inversion of the TDEM data was also conducted along the six transects (Fig. 1). The nonlinear inversion technique (de Groot-Hedlin and ConsTable 1990; Tikhonov and Arsenin 1977) was applied to each one of the transects. This algorithm is based on the 1D laterally constrained (LCI)

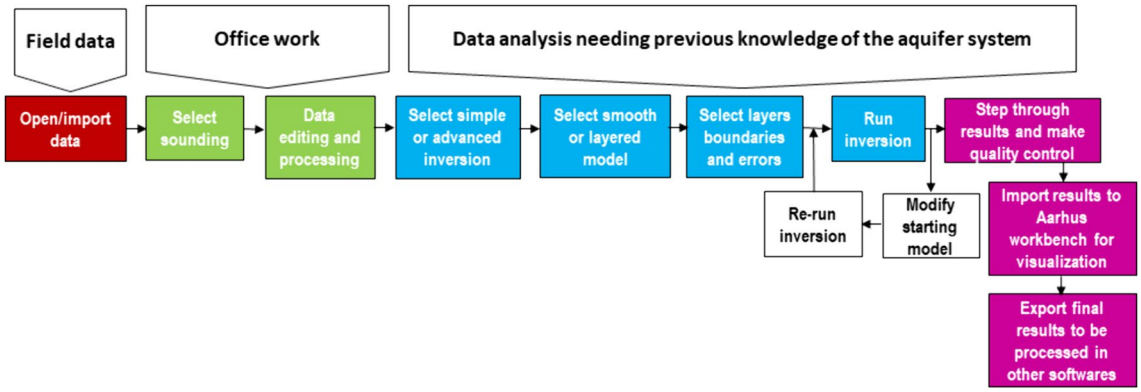

Fig. 2 Flowchart of the 1D smooth and layered inversion conducted using SPIA (Aarhus Geosoftware 2022) and related actions to the Cunene TDEM survey

presented by Monteiro Santos (2004), creating a 2D mesh of blocks according to the TDEM location along each transect (Fig. 3). The constraints are related to the structure of the model. It is imposed a smooth variation of the model around the initial resistivity value. The initial model is an uniform model with a resistivity equal to the average value of the data apparent resistivity, not being possible to impose user-defined constraints, defined from borehole data for instance.

The inverse problem requires an iterative procedure as it involves a nonlinear relationship between model response and model parameters. The logarithm of the block resistivity and apparent resistivity were used as model parameters and data, respectively. The minimization of an objective function allows calculating the correction of the model parameters for each iteration. The objective function used in this work is:

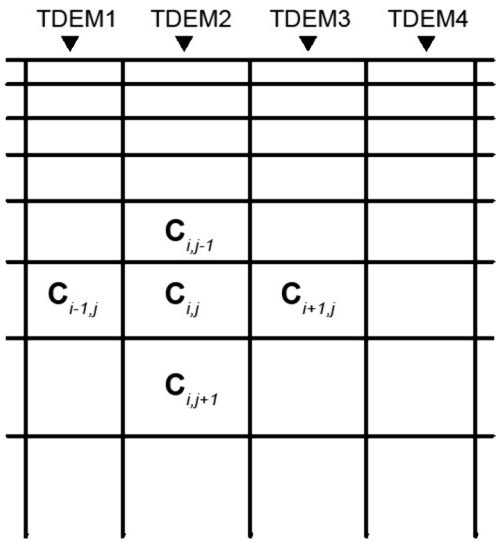

Fig. 3 2D mesh of blocks built according to the TDEM location along each transect. The $\mathbf{C}_{i,j}$ values represent the elements of the roughness matrix $\mathbf{C}$

$$Q = \mathbf{W}_{\mathrm{d}}\left\|\left(\delta\vec{d} - \mathbf{J}\delta\vec{p}\right)\right\|^2 + \lambda^2\mathbf{C}\|\vec{p} - \vec{p}_{\mathrm{o}}\|^2 \tag{2}$$

where $\| \ldots \|$ represents the L_2 norm, $\mathbf{W}_{\mathrm{d}}$ is a diagonal matrix, consisting of the reciprocal of data standard deviations, $\delta\vec{p}$ is the vector containing the corrections to the model parameters and $\vec{p}_{\mathrm{o}}$ is the a priori defined model. $\delta\vec{d} = \ln\left(\frac{\rho_{\mathrm{o}}}{\rho_{\mathrm{c}}}\right)$ is the vector containing the differences between the observed and calculated apparent resistivity in the logarithmic domain. $\mathbf{J}$ is the Jacobian matrix containing the derivatives of the apparent resistivity to the model parameters, also in logarithmic domain. The quantity λ is the damping factor controlling the amplitude of the parameter corrections, whereby the optimum value is empirically determined. The elements of the matrix $\mathbf{C}$ are the coefficients of the values of the roughness in each parameter, which is defined in terms of the neighbors (Fig. 3).

The minimization of Q yields the following normal equation:

$$\left[\left(\mathbf{W}_{\mathrm{d}}\mathbf{J}\right)^{\mathrm{T}}\mathbf{W}_{\mathrm{d}}\mathbf{J} + \lambda^2\mathbf{C}^{\mathrm{T}}\mathbf{C}\right]\delta\vec{p} = -\left(\mathbf{W}_{\mathrm{d}}\mathbf{J}\right)^{\mathrm{T}}\mathbf{W}_{\mathrm{d}}\delta\vec{d} + \lambda^2\mathbf{C}^{\mathrm{T}}\mathbf{C}\left(\vec{p} - \vec{p}_{\mathrm{o}}\right) \tag{3}$$

Equation (3) is solved using a conjugate gradient method ($\mathbf{C}^{\mathrm{T}}$ denotes transposition of matrix $\mathbf{C}$). Once this system of equations is solved, the model parameters are updated and the iteration process finishes when the misfit is reduced to an acceptable value or the number maximum the iterations is reached.

The error between the simulated and measured values is computed for each TDEM sounding using the root mean square error (RMSE), expressed in percent, as following:

$$\mathrm{RMSE} = 100 \bullet \sqrt{\frac{1}{n} \bullet \sum_{i=1}^{n} \frac{\left(d_{\mathrm{obs},i} - d_{\mathrm{sim},i}\right)^2}{\left(d_{\mathrm{obs},i}\right)^2}} \tag{4}$$

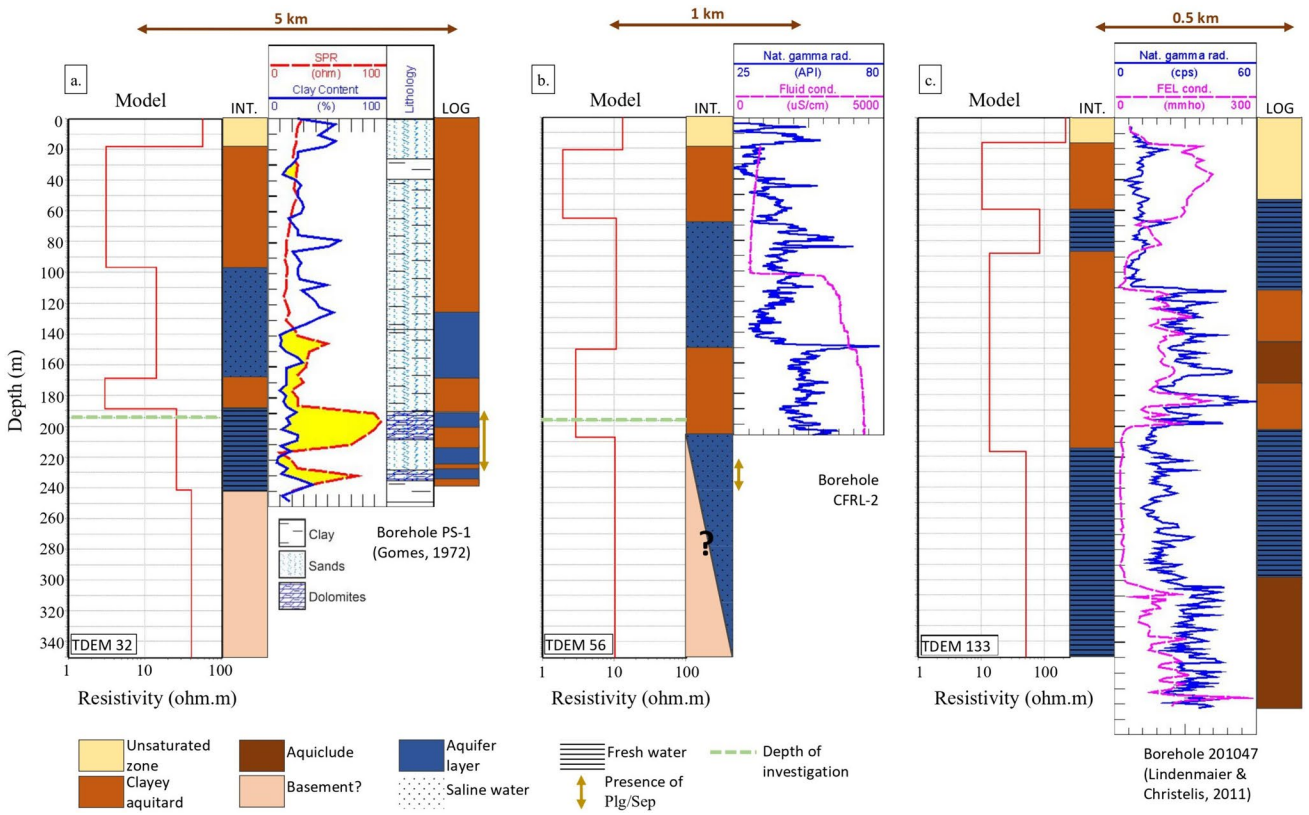

Fig. 4 Results of the 1D inversion of TDEM soundings and corresponding auxiliary data (location on Fig. 1): (**a**) 32: DOI = 194, DR = 0.94; (**b**) 56: DOI = 197, DR = 0.75; and (**c**) 133 DOI = 497, DR = 0.07). INT.: hydrogeological interpretation of the TDEM inversion. Nat. Gamma Rad.: Natural Gamma Radiation log. SPR: Single Point Resistance log. Fluid Cond.: Fluid Conductivity log. FEL: Focused Electrical Resistivity of the rock host

where d_{obs} is the measured value, d_{sim} is the simulated value and n is the number of data points.

Results and interpretation

Results were approached in two different ways. For the 1D inversion results, it was important to have a local overview for each site, to test the existence of local anomalies and to evaluate the possibility in the near future of using single loop inverted data in groundwater resources management at the basin scale. In sectors considered relevant to understand the aquifer system geometry, boreholes data were used to constrain the 1D TDEM inversions. This calibration is important as in some areas, the 1D TDEM data provide the only information available to support borehole sitting decisions. On the other hand, the quasi-2D inversions gave an overview of the basin geoelectrical characteristics that allowed a more detailed assessment of the basin geometry.

1D inversion

All 112 TDEM soundings acquired in this study were inverted, obtaining DR (Eq. 1) of the inversion model varying from 0.12 to 2.54 using the smooth inversions and 0.05 to 1.51 using the layered inversions. Globally, results were considered satisfactorily, since 72 and 81% were below 1 for the smooth and layered inversions, respectively.

The results from three key sectors with relevant data such as borehole logs and/or well logging are presented in Fig. 4 and discussed.

Môngua sector

The layered inversion of TDEM 32 (Fig. 1) comprised six layers and its DR was 0.94. The inversion was constrained using the information of the borehole PS-1 (Gomes 1972), located near the Môngua village (Fig. 1). This borehole is 250 m deep with four productive layers located at 128–170, 192–201, 215–225 and 228–235 m (Fig. 4a). The single point resistance (SPR) log detected the presence of these

aquifer layers and indicated that the shallowest layer has higher salinity, since the measured resistance is considerably lower than in the three deepest aquifer layers (Fig. 4a). The clinoptilolite-rich layer (marker of the intermediate, saline aquifer) is located between 130 and 172 m deep, in fine to medium sands, while the Plg/Sep clays-rich layer (indicator of the deep aquifer) is located between 190 and 230 m, in consolidated sandy dolomites (Gomes 1972). Total dissolved solids (TDS) of the water of the four productive layers mixed together is relatively high (3,541 mg/L), as well as the electrical conductivity (4,500 µS/cm), while its pH is alkaline (7.9). The hydrochemical facies is sodium-sulfate, with a high chlorides level.

The intermediate, saline aquifer is identified in the TDEM layered inversion between 100 and 170 m depth, with an electrical resistivity of 14 Ω.m, while it was recognized between 128 and 170 m in the borehole. The deeper layers were also identified in the 1D TDEM inversion between 190 and 240 m, with an electrical resistivity of about 40 Ω.m, although the inversion at this depth is quite uncertain, i.e. just below the depth of investigation (DOI). However, this seems plausible, since a passive seismic station located 4 km away indicates a basement depth of about 330 m (Carvalho et al. 2024). This specific site was also studied by Ramalho et al. (2023b), where the electrical resistivity obtained from the 3D geoelectrical model matches perfectly either with the SPR and clay content logs or the 1D TDEM layered inversion depicted in Fig. 4a.

Namacunde sector

The layered inversion of TDEM 56 comprised five layers with a DR of 0.75. It was conducted near three boreholes drilled by the private company CFRL, Angola. These boreholes (Fig. 1) are located a few meters away from each other and are representative of the hydrogeological scenarios in Cunene: i) CFRL-1 is very shallow with depth < 60 m and unproductive; ii) CFRL-2 is 210 m deep, with groundwater electrical conductivity ca. 4,500 µS/cm and not exploited due low productivity and high clay content, particularly below 150 m, as evidenced by the natural gamma ray log (Fig. 4b., next to fluid electrical conductivity); and iii) CFRL-3 has a total depth of ca. 300 m and screens at possible depths between 220 and 280 m; groundwater has an electrical conductivity of ca. 5,000 µS/cm, being currently under exploitation to produce cement, which requires artificial desalination. As such, in this low electrical resistivity environment, the 1D inversion is quite uncertain. Although the existence of a saline, intermediate aquifer was recognized, its thickness is overestimated and there is high uncertainty in the distinction between saline aquifers from clayey layers without the assistance of a natural gamma ray log. The Plg/Sep layer was identified at a depth between 227 and 243 m (Gomes 1972), which agrees with the screen depth of borehole CFRL-3.

Eastern sector

The layered inversion of TDEM sounding 133 comprised six layers with a DR of 0.07. It was carried out near borehole 201047 (Lindenmaier & Christelis 2011), located in Namibia (Fig. 1). This borehole is 380 m deep and features well logging data (natural gamma ray and short/long range electrical conductivity). There was a very good correspondence between the hydrogeophysical interpretation of the 1D layered inversion of the TDEM 133 and the data of the borehole 201047 depicted in Fig. 4 c. Two aquifer layers of fresh water were recognized, between 60 and 88 m and between 216 and 350 m, with electrical resistivity of 84 and 50 Ω.m, respectively. Note that in this more resistive environment, the DOI is much deeper (497 m) than the one of the inversions of TDEM soundings 32 and 56 (DOI of 194 and 197 m respectively), indicating a better resolution of the inversion at depth. The passive seismic station located near this TDEM indicates a basement depth of about 375 m (Carvalho et al. 2024).

Quasi-2D inversion

The results of the quasi-2D inversions are presented for each transect in Fig. 5, using the electrical resistivity ranges defined in Table 1. All transects share the same vertical and horizontal scales, as well as the same electrical resistivity color scale, for direct comparison. In complement, the transects were also symbolized using a classical representation with a logarithmic detailed color ramp. Their georeferencing allowed a 3D visualization that evidences the geometry of the geological basin (Fig. S2 of the ESM).

The statistical distribution of the RMSE of the quasi-2D inversions (Eq. 4) is shown in Fig. S3 of the ESM while individual values are listed in Table S1 of the ESM and the fitting of the observed and simulated signal curves is shown in Figs. S4 to S9 of the ESM. As the distribution is positively skewed (min: 2.5%, median: 6.8% and maximum: 33.8%), the RMSE was classified into four classes using the geometric interval method (see explanations in the caption of Fig. S3 of the ESM). To quickly visualize the reliability of the TDEM inversion, the label of each TDEM sounding in Fig. 5 was represented with a color that represents the RMSE class: dark green < (g_1 = 4.8%) < green < (g_2 = 9.2%) < orange < (g_3 = 17.7%) < red, where g_1, g_2 and g_3 are the geometric interval limits. Globally, the RMSE of the inversion is acceptable since 75% of the RMSE is less than 10.7% (3rd quartile). The RMSE is higher in areas with higher

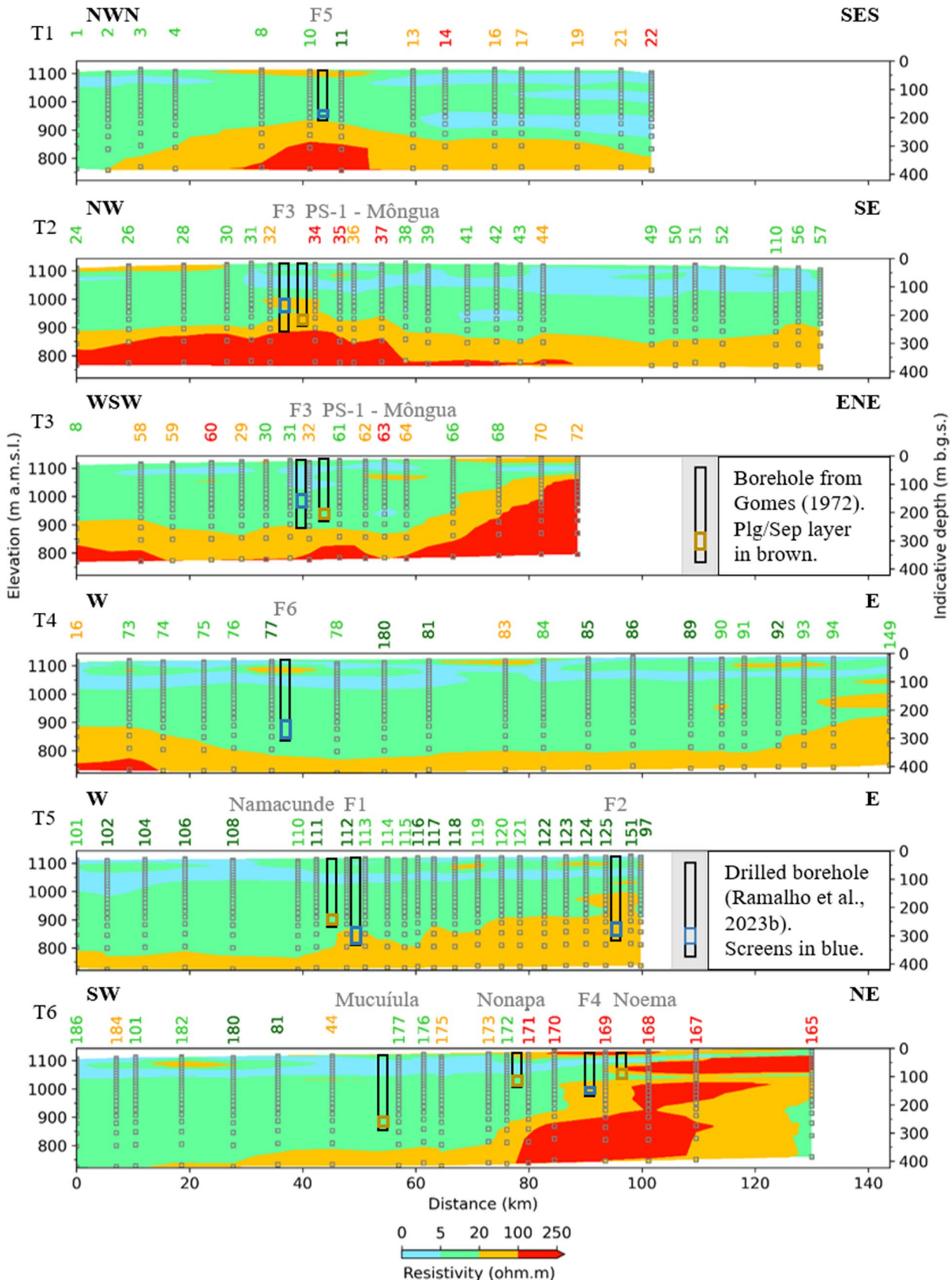
T1
NWN
F5
SES
T2
NW
F3 PS-1 - Môngua
SE
T3
WSW
F3 PS-1 - Môngua
ENE
T4
W
F6
E
T5
W
Namacunde F1
F2
E
T6
SW
Mucuíula
Nonapa
F4 Noema
NE
Elevation (m a.m.s.l.)
Indicative depth (m b.g.s.)
Borehole from Gomes (1972). Plg/Sep layer in brown.
Drilled borehole (Ramalho et al., 2023b). Screens in blue.
Distance (km)
Resistivity (ohm.m)
0 5 20 100 250

◂**Fig. 5** TDEM transects T1 to T6. The horizontal scale corresponds to the distance between the TDEM soundings (the first TDEM station in each transect corresponds to the value 0). The colored, vertical label at the top indicates the ID of the loop, while the circles correspond to the signal measurement. The color corresponds to the RMSE class (dark green < (g_1 = 4.8%) < green < (g_2 = 9.2%) < orange < (g_3 = 17.7%) < red, where g_1, g_2 and g_3 are the geometric interval limits). F3*: as borehole F3 was not drilled, the indicated values of top and bottom screens and total depth are the ones estimated (Table 2). a.m.s.l.: above mean sea level. b.g.s.: below ground surface

electrical resistivity contrast, e.g. at the northeast border of the basin, visible on transect 6 (T6). This behavior was expected since it is inherent to the inversion method. Indeed, the transect T6 includes, in the center of the basin, detrital, pseudo-horizontal and relatively continuous layers from the Cenozoic that laterally pass to heterogeneous, highly deformed substratum from the Precambrian at the northeast border. As the damping factor (Eqs. 2 and 3), which controls the degree of lateral constraint in the inversion (in other words, the importance of adjacent TDEM soundings in the inversion of the centrally located TDEM sounding), was the same for all transects (0.3), it cannot accommodate both geophysical settings.

The main observations that can be made on the transects are:

1 A shallow layer, i.e. in the first one hundred meters of the subsurface, with very low resistivity (1 Ω.m) crosses the entire length of the transect, with some discontinuities. It likely corresponds to a clay aquitard. Along T1, a shallow layer north of Xangongo (TDEM soundings 1 to 4) is identified, while at South of Ombala yo Munguo (TDEM soundings 13 to 22) three overlying layers are identified up to 200 m deep.
2 Above the low resistivity layer detected in the previous point, lenticular layers of resistivity ranging between 20 and 100 Ω.m may correspond to lenticular, perched aquifers, which is particularly evident in transects T3, T4 and T5. These aquifers are recharged by rainwater during the rainy season and often dry completely in the dry season (Hamutoko et al. 2019). Some shallow boreholes producing fresh water are abundant in the study area, abstracting groundwater from these perched aquifers. However, the relatively circumscribed three-dimensionality of these lenticular bodies of reduced size, corresponding to paleochanas and paleoecangos, leads to a high number of dry drill-holes in the vicinity, relatively near the productive wells. Moreover, these perched aquifers may also contain mineralized water, sometimes unfit for human consumption.
3 The basin shows, in most of its extension, intermediate resistivity between 5 and 20 Ω.m. It corresponds to interbedded layers that may contain thin aquifers, most of them with probably high salinity, or clayey sands. The overlapping of resistivity ranges between the intermediate aquifer of high salinity and clayey sandy layers makes the interpretation and estimation of the depth of the intermediate aquifer difficult.
4 The deepest part of the basin shows resistivity higher than 100 Ω.m which corresponds to the basement (pre-Cenozoic rocks, in this case).
5 Across the basin, a layer ca. 50 to 100 m thick and resistivity between 20 and 100 Ω.m marks the transition between the layer 5–20 Ω.m and the basement (> 100 Ω.m). This layer can be an effect of the inversion algorithm and/or indicate aquifer layers, containing low to intermediate mineralized groundwater. 1D inversion results are in this case of utmost importance.
6 The structure of the basin is highlighted by the evidence of its lateral borders. The E-NE edge of T3 shows the shallowing of the basement, while the low resistive Cenozoic deposits are reduced to a few tens of meters. Along T4, this is also observed in both edges of the transect: between TDEM soundings 16, 73 and 74 to the west and between TDEM soundings 93, 94 and 149 to the east. Along T6, collapsed blocks are observed, that extend between TDEM soundings 186 and 173, 173 and 169 and 170 to 165, the latter featuring a reduced Cenozoic basin thickness. This transect clearly indicates the eastern boundary of the basin, defined by a staircase structure of collapsed blocks separated by faults, certainly of normal type (horst and graben structure).
7 It is also possible to detect horsts in the depressed sections of the basins: the high resistivity (higher than 100 Ω.m) section at depth in T1, visible between TDEM soundings 8 and 11, can correspond to a structural horst, aligned with a similar structure in T2, observed between its TDEM soundings 32 to 37, and depressed areas at south.

The resistivities from the 3D geoelectrical model (Ramalho et al. 2023b) were extracted along the W-E transects T4 and T5 (Fig. 6). There is very good agreement between the VES and TDEM transects, all of them excellently depicting the structure of the geological basin, particularly the shallow conductive layer and blocks showing the structure in horst and graben, as well as the edges of the basin. However, the VES transects show a lower DOI and the thickness of the low resistivity (<5 ohm.m) layer appears relatively larger.

The electrical resistivities of the transect C (Lindenmaier et al. 2014) between TDEM C-330 and C-600 (Fig. 1) are shown in Fig. 7. It is parallel to transect T5, being located 10–15 km to the south. There are some notable differences between both transects. In transect C, electrical resistivities compatible with the basement are not observed, since the

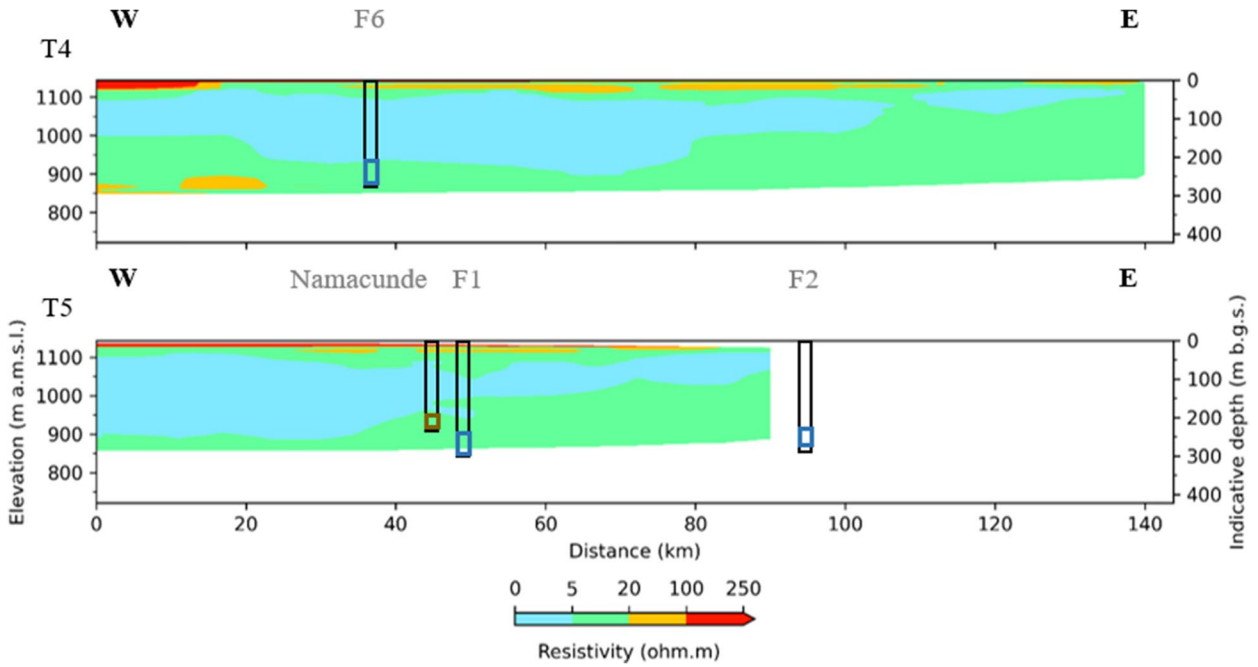

Fig. 6 Transects extracted from the 3D geoelectrical model (Ramalho et al. 2023b). The horizontal scale corresponds to the distance between the VESs (the first VES station in each transect corresponds to the value 0). a.m.s.l.: above mean sea level. b.g.s.: below ground surface

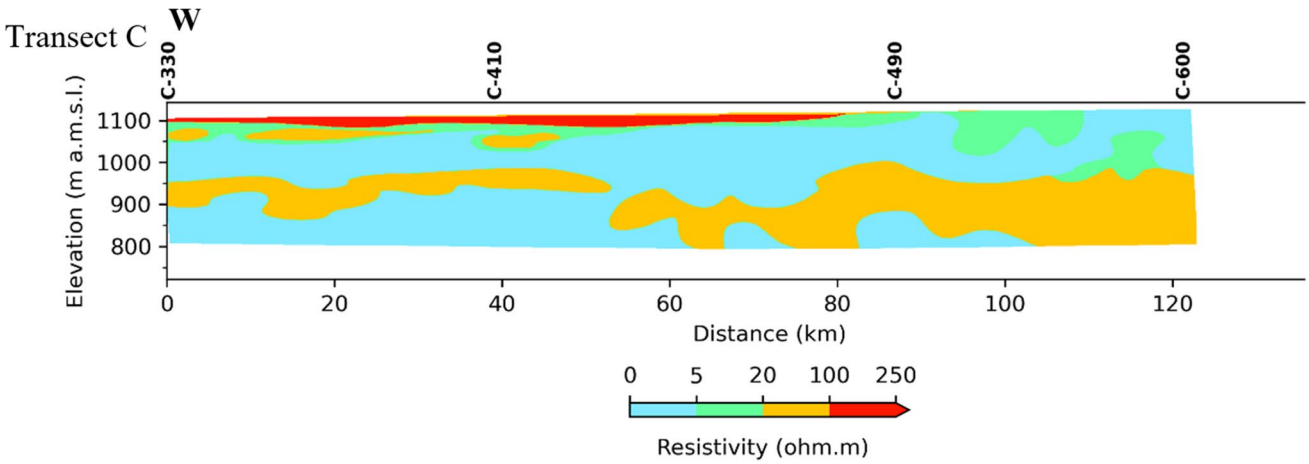

Fig. 7 Electrical resistivity inferred from the TDEM transect C adapted from Schildknecht (2012). The horizontal scale corresponds to the relative distance between the TDEM soundings (the first TDEM station in each transect corresponds to the value 0). The vertical label, in bold at the top, indicates the ID of the loop (Fig. 1). a.m.s.l.: above mean sea level. b.g.s.: below ground surface

bedrock is probably located deeper than the DOI in that particular area, which confirms the deepening of the geological basin towards the southeast direction. The most important characteristic of this transect is the presence of a layer with intermediate resistivity (20–100 Ω.m), in the middle of the low resistivity range (< 5 Ω.m). The intermediate resistivity layer is at a depth between 150 and 200 m in the west, while it is thickening at its base in the east direction, reaching a depth of 300 m. This intermediate resistivity layer may be interpreted as the deep aquifer layer, confined by clayey layers of low resistivity. Note that in the east, this layer is becoming much shallower, as observed by Lindenmaier et al. (2014) and Schildknecht (2012), corresponding to the mapped freshwater aquifer.

Boreholes siting

The six transects of Fig. 5 were analyzed, together with the information provided by Gomes (1972), to prepare a drilling campaign and to site six boreholes (Ramalho et al. 2023a)

Table 2 Estimated and observed top and bottom of the deep aquifer and total depth of the borehole. Estimated values were derived by analysis of electrical resistivity transects shown in Fig. 4 whereas observed values were obtained during a drilling campaign executed within the scope of PLANAGEO (Ramalho et al. 2023a). The error was computed using the following formula to obtain the deviation of the observed value to the estimated value: 100×(observed-estimated)/estimated. ND: not drilled

Borehole ID	Aquifer top			Aquifer bottom			Total depth			EC of the water (µS/cm)
	Estimated (m)	Observed (m)	Error (%)	Estimated (m)	Observed (m)	Error (%)	Estimated (m)	Observed (m)	Error (%)	
F1	215	240	12	315	288	-9	325	300	-8	2370
F2	130	223	72	180	281	56	230	294	28	476
F3	125	ND		175	ND		250	ND		ND
F4	135	128	-5	185	152	-18	285	158	-45	11,100
F5	110	125	14	180	143	-21	250	147	-41	9640
F6	250	190	-24	300	254	-15	350	258	-26	2340
Min	110	125	-24	175	143	-21	230	147	-45	476
Median	133	190	12	182.5	254	-15	267.5	258	-26	2370
Max	250	240	72	315	288	56	350	300	28	11,100

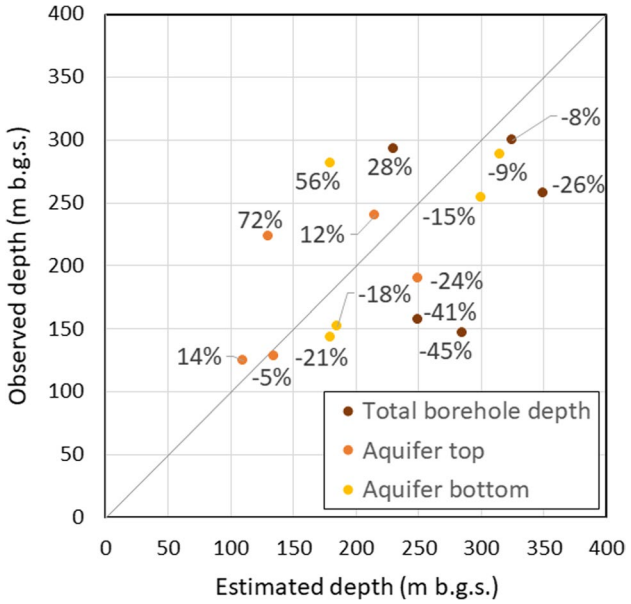

Fig. 8 Error between estimated and observed top and bottom of the deep aquifer and total depth of the boreholes (see formula of error in the caption of Table 2)

to be distributed across the basin and to include important sectors to ascertain the aquifer system geometry.

Boreholes F1 and F2 were positioned on T5. The borehole located near Namacunde (Gomes 1972) shows the layer of Plg/Sep at a depth between 227 and 243 m (see Fig. 4b). It corresponds to a zone of resistivity between 5 and 20 Ω.m, close to a structural high with a resistivity of ca. 30 Ω.m, between the TDEM soundings 111 and 114. The borehole F1 was sited between TDEM 112 and 113, with a total depth of 325 m, intersecting an aquifer between 215 and 315 m (Table 2). F2 was sited further to the east with a total depth of 294 m, whereas the expected depth of the basement was 230 m. It was screened to a zone with a resistivity between 30 and 50 Ω.m and shallow depth (~ 100 m). This area is located within the freshwater zone defined by Lindenmaier et al. (2014).

Borehole F3 was sited using T2 and T3 and the PS-1 Môngua borehole (Gomes 1972), which indicates that the Plg/Sep layer is between 190 and 230 m deep, which corresponds to a higher resistivity zone (20–30 Ω.m) in T2 and may indicate an aquifer zone between 125 and 175 m depth, containing groundwater with relatively low mineralization.

The transect T6, where borehole F4 was sited, benefits from three borehole logs studied by Gomes (1972) with Plg/Sep layer depths, from SW to NE, at 258–283 m depth (Mucuíula), 100–125 m (Nonapa) and 93–106 m (Noema). While these depths are consistent with the transect regarding the Mucuíula and Noema boreholes, i.e., the Plg/Sep layer lies near the basin/basement boundary, in the Nonapa borehole, this layer is at a much greater depth, just below the clay

aquitard. This incoherence may be due to a borehole georeferencing error that, in this zone of abrupt changes, would explain the elevated position of this layer at this location, as well as the high RMSE of the inversion, as previously discussed in the quasi-2D inversion section. F4 was drilled to a shallow depth (total depth of the borehole ca. 285 m), near TDEM sounding 169, where a zone of electrical resistivity between 30 and 50 Ω.m was identified and interpreted as the presence of an aquifer layer containing groundwater with relatively low mineralization.

Borehole F5 was sited on T1, above the previously identified horst (structural high with higher resistivity > 100 Ω.m), between TDEM soundings 10 and 11, where a zone of intermediate resistivity (between 20 and 100 Ω.m) may indicate an aquifer zone with lower mineralized water at 110–180 m depth.

Borehole F6 was sited close to TDEM 77 on T4, expecting that the resistivity zone between 20 and 100 Ω.m, at 250–300 depth, could correspond to the deep aquifer.

The estimations based on the TDEM transects analysis of the total depth of the boreholes and of the top and base of the deep aquifer are compiled in Table 2. The real depths observed during drilling are also reported and plotted against the estimated values in Fig. 8. Note that only 5 boreholes were drilled, as the F3 site was not accessible due to the presence of land mines.

Discussion

Contribution of TDEM to the hydrogeological conceptual model

The geometry of the geological basin is well depicted in the TDEM transects that clearly show the edges, the deepening in southeast direction and the overall graben and horst structure. A complementary study, based on tectonic analysis and passive seismic geophysical method, also confirmed these observations (Carvalho et al. 2024). The age of the tectonic features seems to be pre-Upper Kalahari Subgroup, since only the deposits of the Lower Kalahari Subgroup are affected by faults. The most important structure detected has an ENE-SWS direction, passing north of Ondjiva. This feature, as well as the general geometry of the basin, were also evidenced in the 3D geoelectrical model (Ramalho et al. 2023b) and from aeromagnetic data (Fig. S10 of the ESM). This ENE-SWS structure delimitates a collapsed block in the south of the study area, characterized by very low electrical resistivity, which may indicate saline/brackish aquifer and/or high clay mineral content. It is not clearly visible in the TDEM transects, except in T2, in which the high resistivity range (> 100 Ω.m) related to the basement disappears towards the south of TDEM sounding 44, indicating that the basin is deepening. Moreover, another structure interpreted as a normal fault (Carvalho et al. 2024), also with a ENE-SWS direction and passing south of Môngua, is also clearly detected in T1, between TDEM soundings 11 and 13, and T2, between TDEM soundings 37 and 38. This structure is important as it explains the presence of the Lower Kalahari Subgroup at lower depths in the sector located north of this tectonic structure (corroborating with outcrops along the Cunene River and near Cahama on Fig. 1). The difference in elevation of these two main blocks may also explain the difference in groundwater salinity between these two blocks, since the tectonic structure may be ultimately responsible for different depositional environments.

In addition to the structural control on the N-S direction of the basin geometry, there is also clear evidence of tectonic controls in the E-W direction, namely in the Cuvelai region (Carvalho et al. 2024, Represas et al. 2021). This staircase structure resulted in depressions oriented NW-N to E-SE and dipping towards SE-S, which may have exerted a strong influence in the control of the development of the paleo-fluvial systems and thus the deposition of the Lower and Upper Kahari Subgroups. This structural control is evident in the two E-W transects T4 and T5, where a clear rising of the basement in the east was detected. This zone is the western limit of the freshwater area defined by Lindenmaier et al. (2014), which is confirmed by the relatively low groundwater electrical conductivity from boreholes F1 and F2 (2370 and 476 µS/cm, respectively, as shown in Table 2). The lenticular body between 100 and 200 m depth visible in all transects, with an electrical resistivity between 20 and 100 Ω.m, may thus correspond to the aquifer layer containing freshwater. This area could be the transition between the deposits of the Cubango and Cunene megafans, controlled by a N-S horst and by the presence of the Onimwandi dyke swarm (Miller 1992, 2008), as referred in Department of Water Affairs (1991), although they concluded that "the effect of the Onimwandi dyke swarm on an apparent groundwater transition zone could not be evaluated but appears to be minimal, as the transition zone occurs to the west of Eenhana [Namibia] which is a further 2 km west of the edge of the dyke swarm". This structure is clearly identified on the aeromagnetic map (Fig. S10 of the ESM) and should be the target of dedicated structural and geophysical studies, such as seismic surveys to identify the relationship between the deposition settings and the dyke swarm.

As seen from the presented analysis and interpretation of T4 and T5, delimitation of the KOH in Angola using electrical properties and the TDEM results must be treated with caution; in fact, both T4 and T5 show an increase in electrical resistivity in the east, being more pronounced in the southern transect (T5). These variations are also visible in the 3D geoelectrical model (Ramalho et al. 2023b) and may reflect the basic difference between KOS and KOH related

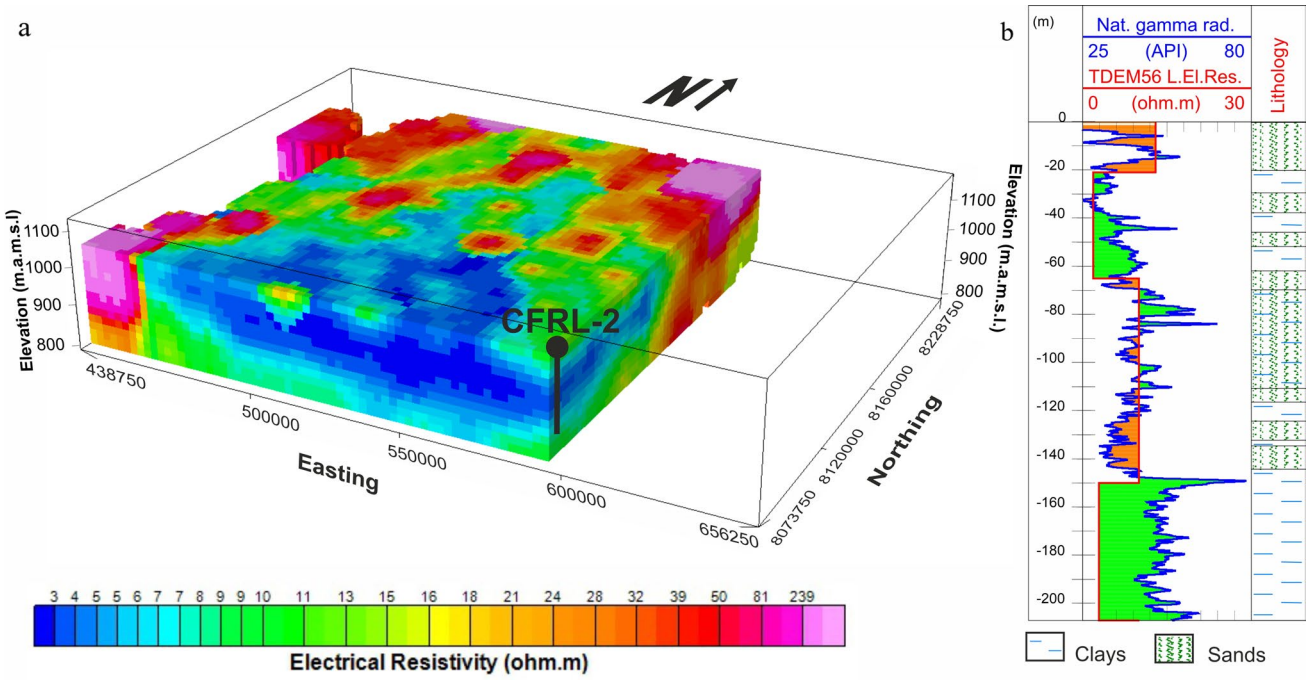

Fig. 9 (**a**) Projection of the CFRL-2 borehole in the 3D geoelectrical model (Ramalho et al. 2023b); (**b**) Natural gamma radiation log of CFRL-2 and electrical resistivity model from a layered inversion of TDEM sounding 56, with the lithological log derived from their joint interpretation

to more favourable groundwater quality, i.e., less mineralized groundwater.

Geophysics to support borehole siting

The deviation of the observed values of aquifer top and bottom depths with the values estimated using the quasi-2D TDEM inversions is globally low (Table 2 and Fig. 8), with a particularly good agreement with the top and bottom depths of the deep aquifer. The largest errors are related to borehole F2, since the target layer of resistivity 20–100 Ω.m at depth 130–180 m featured saline water. The productive layer with freshwater was reached between 223 and 281 m. Moreover, F2 was not drilled adjacent to the T5 transect as the drilling rig could not travel over the sandy ground (Fig. 1). In addition, no data regarding the depth of the Plg/Sep marker (Gomes 1972) was available for this area (Fig. 1). Indeed, this clay marker was a valuable indicator, confirming that natural gamma ray borehole logs were crucial to calibrate the TDEM data and properly interpret the inversion results. As referred to in Ramalho et al. (2023b), a decrease of the natural gamma radiation log values can be a marker of the Plg/Sep layer due to the absence of K^+ mineralogy, as opposed to K^+-rich clays that compose the lithological columns either from KOS or KOH, namely clinoptilolite, montmorillonite and illite.

On the other hand, making the best use of the scarce available information is a challenge for hydrogeological research in Cunene. A good working basis based on the electrical properties of the geological formations was provided by the 3D geoelectrical model based on VES from the 1960s (Ramalho et al. 2023b) and 1D TDEM results. Within the framework of a wider research program, this information should be correlated with natural gamma radiation logs measured in existing deep and cased boreholes without pumps installed. Although scarce, the information they supply, jointly interpreted with the 1D TDEM results, can improve insights and obtain greater information from the deeper aquifers of both KOS and KOH aquifer systems, especially in areas that were not covered by the 1966/67 VES survey of Nascimento et al. (1966, 1967). That is the case for three CFRL boreholes, previously described, located in Santa Clara, ca. 10 km away from the Namibian border (Fig. 1). Nevertheless, the correspondence of the electrical resistivities ranges of the hydrogeological domains from Table 1 and the 1D layered inversion of TDEM sounding 56, which is distanced ca 200 m from the CFRL boreholes, can lead to misinterpretations. This is because sands containing saline water and/or clays can have similar electrical resistivities (Sharma 1997; Telford et al. 1990) which can lead to the misidentification of productive zones and installation of well screens at unsuitable locations. In these cases, the use of natural gamma radiation logs in cased boreholes can be an effective way to distinguish the several hydrogeological environments present in the area. This case is illustrated in the joint

interpretation of the layered 1D inversion of TDEM 56 and the natural gamma radiation log of the cased borehole CFRL-2 (Fig. 9). While it can be confirmed that a significant part of CFRL-2 intersects thin intercalations of sandy and clayey formations, the low resistivity values can also be related either to highly mineralized groundwater and/or clayey formations with very low to almost negligible permeabilities (Custodio and Lamas 1996). The layered inversion of the electrical resistivity of TDEM sounding 56 (Fig. 9b) individualize high electrical resistivity layers that correlate with low gamma radiation layers, from 0–20, 30–35, 90–100, 65–70 and 122–142 m. However, most of the screens were located below this depth, leading to the abandonment of the well and to the drilling of the deeper CFRL-3 well that is currently in use for groundwater abstraction.

Recommendations for future studies

There are still two main types of uncertainty present within the interpretation of geoelectrical and electromagnetic data that do not allow for the distinction of: (i) low resistivity zones that may correspond to a clay layer, saline aquifer or clayey sands containing saline/brackish water at intermediate depths (100–200 m); and (ii) intermediate resistivity zones that may correspond to the transition towards the basement or deep aquifers with low groundwater mineralization. As such, direct interpretation of the electrical resistivity properties either from VES or TDEM surveys may be insufficient to identify the best screen location when drilling deep wells in Cunene. In most cases, this is the only information available. Therefore, to improve the interpretation of the TDEM results, and to successfully break the decades of suspended hydrogeological progress in Cunene, several procedures should be implemented:

1 To plan higher resolution TDEM surveys (i.e. shorter distance between successive TDEM soundings) in areas of interest (along the T5 transect for instance) with complementary parallel transects, to support the development of 3D TDEM models in the near future;
2 To use the inventory of boreholes in the Cunene province to conduct joint interpretation of natural gamma radiation logs in drilled wells in the Cunene province with 1D inversions of TDEM soundings. This procedure will constrain the calibration mesh and provide a greater distinction between clayey layers and the small aquifers at intermediate and deeper depths associated with the KOS and KOH aquifer systems in each area. This methodology can be applied across the basin, where unused boreholes are available.
3 To promote the regular use of TDEM surveys to guide groundwater borehole drilling, with the appropriate loop configuration to reach the target depth of investigation required for aquifer characterization, especially in areas that have not previously been studied within a hydrogeological context.
4 To detect the perched aquifer in the shallow layer (KOH-0 or KOS-0), it is recommended to use adjust TDEM system settings for shallow depths (40 m side loop and small RC-5 antenna). Other complementary methods, such as electrical resistivity tomography (ERT) or magnetic nuclear sounding (MRS) would also support interpretations. ERT is suitable for detecting and mapping the perched aquifers of the KOS-0 and KOS-0 aquifers (Hamutoko et al. 2019), as they are relatively shallow (< 100 m) and there is a large resistivity contrast with the surrounding rocks. Within hydrogeophysics, the MRS is the unique method that is directly and exclusively sensitive to the presence of groundwater since it measures the signal originating from the hydrogen protons present in the water molecule (Legchenko et al. 2004; Lubczynski and Roy 2007). The MRS method has been applied in detrital sedimentary basins with multilayer aquifer systems with low electrical resistivity, in the Delft area of the Netherlands (Lubczynski and Roy 2004) and Waalwijk (Lubczynski and Roy 2003), and in the Paris Basin, France (Vouillamoz 2003 in Vouillamoz et al. 2007). However, Lubczynski and Roy (2003, 2004) reported difficulty in applying the MRS method to fractured aquifers in Southern Africa (Botswana) due to the low values of the Earth's magnetic field and the presence of natural electromagnetic noise caused by frequent thunderstorms prevented acquisition of a valid MRS signal.

Conclusions

TDEM soundings were collected along transects in the Kalahari Cenozoic sedimentary basin in the Cunene Province. Their quasi-2D inversion allowed to elaborate electrical resistivity 2D transects that showed alternating layers of low (< 20 Ω.m) and intermediate resistivity (20–100 Ω.m), overlying a relatively higher resistivity layer (100 Ω.m) corresponding to the basement. There is a very good agreement between an existing 3D geoelectrical model (Ramalho et al. 2023b) and, together, these models allowed for the depiction of the basin geometry and interpretation of its tectonic control. Moreover, the interpretation of these models allowed for the identification of the three aquifers of the Kalahari system, with special emphasis on the intermediate and deep aquifers. Low resistivities indicated the presence of clayey layers and clay matrix of the detrital deposits with a moderately mineralized groundwater content. At greater depth,

the intermediate resistivities are associated with the basin-basement transition (lower Kalahari) and the presence of the deeper aquifer, which is consistent with the presence of the Plg/Sep layer (Gomes 1972). Finally, it is crucial to note that the water resource provided by the deep aquifer has a very low to negligible recharge rate (Himmelsbach et al. 2018; Wallner et al. 2017). As such, further studies must be conducted to accurately map the location of the freshwater zones and to implement a protection management plan with a legal framework to explore this valuable and finite resource for the Cunene Province.

Supplementary Information The online version contains supplementary material available at https://doi.org/10.1007/s10040-024-02822-x.

Acknowledgements The authors wish to thank Roland Bäumle, Uwe Meyer and Seinab Bohsung, from the Bundesanstalt für Geowissenschaften und Rohstoffe (Geological Survey of Germany, BGR) for their collaboration in hydrochemistry analysis, Bruno Barros for creating the 3D TDEM visualization diagram (Fig. S2 in the ESM) and José Feliciano Rodrigues from Laboratório Nacional de Energia e Geologia for his review and valuable suggestions on the geology section.

Funding Open access funding provided by FCT|FCCN (b-on).

Declarations

Conflict of interest On behalf of all authors, the corresponding author states that there is no conflict of interest.

References

Aarhus Geosoftware (2022) SPIA - ground based TEM software. https://www.aarhusgeosoftware.dk/aarhus-spia-tem. Accessed 17 Sept 2023

Auken E, Christiansen AV, Jacobsen BH, Foged N, Sørensen KI (2005) Piecewise 1D Laterally constrained Inversion of resistivity data. Geophys Prospect 53:497–506. https://doi.org/10.1111/j.1365-2478.2005.00486.x

Auken E, Christiansen AV, Westergaard JA, Kirkegaard C, Foged N, Viezzoli A (2009) An integrated processing scheme for high-resolution airborne electromagnetic surveys, the SkyTEM system. Explor Geophys 40:184–192. https://doi.org/10.1071/EG08128

Bittner Water Consult (2006) Desk Study Report: Cuvelai-Etosha Groundwater Investigation. Technical report, Technical Cooperation Project BGR / DWAF

Carvalho H, Fernandes FC, Pereira E (1973b) 'Notícia explicativa da carta geológica de Angola à escala 1:250 000. Folha Sul D-33/U – Chibemba', Direcção Provincial dos Serviços de Geologia e Minas. Província de Angola, Portugal, p 27

Carvalho H (Coordinator) (1982) Carta Geológica de Angola à escala 1:1.000.000', Pub. Inst. Inv. Cient. Tropical, Lisboa. Investigações Ultramar (4 sheets)

Carvalho H, da Motta Marques JM, Fernandes FC (1973a) Carta geológica de Angola à escala 1:250 000. Folha Sul D-33/U – Chibemba', Direcção Provincial dos Serviços de Geologia e Minas. Província de Angola, Portugal

Carvalho JG, Alves D, Borges J, Caldeira B, Cordeiro D, Machadinho A, Oliveira A, Ramalho E C, Máximo J, Llorente JM, Ditutala M, Rodrigues JF, Carvalho C, Labaredas J, Garcia-Lobon JL, Manuel J (2024) Depth estimation of pre-Kalahari basement in Southern Angola using seismic noise measurements. J Appl Geophys. https://doi.org/10.1016/j.jappgeo.2024.105498

Christelis G, Struckmeier W (eds) (2011) Groundwater in Namibia - an explanation to the Hydrogeological Map, unrevised 2nd edn. Technical Cooperation Project "HYMNAM", prepared by DWA, GSN, NAMWATER & BGR, Windhoek, 128 p

Custodio E, Lamas MR (1996) Hidrologia Subterranea, Ediciones Omega

de Groot-Hedlin CD, Constable SC (1990) Occam's inversion to generate smooth, two-dimensional models from magnetotelluric data. Geophysics 55(12):1613–1624. https://doi.org/10.1190/1.1442813

Department of Water Affairs (1991) Final report - phase 1 groundwater investigations Eastern Owambo, vol. 1 report, Technical report 2710/4/G2, Republic of Namibia

Dill HG, Kaufhold S, Lindenmaier F, Dohrmann R, Ludwig R, Botz R (2013) Joint clay-heavy-light mineral analysis: a tool to investigate the hydrographic-hydraulic regime of Late Cenozoic deltaic inland fans under changing climatic conditions (Cuvelai-Etosha Basin, Namibia). Int J Earth Sci 102(1):265–304. https://doi.org/10.1007/s00531-012-0770-7

Escuder-Viruete J, Gumiel J, Iglesias-Martínez M, Goicoechea P (2018) Carta Geológica de Angola à escala 1:250 000, folha Sul E-33/CI (Cahama) e Memória Explicativa (2ª edição)'. UTE (IGME, LNEG, Impulso) - IGEO, Luanda, 260 pp

Feio M (1966) A Evolução do Relevo da Bacia Endorreíca do Cuanhama (Angola). Finisterra-Revista Portuguesa De Geografia I(1):33–59

Feio M (1970) O rio Cunene. Estudo Geomorfológico'. Finisterra-Revista Portuguesa de Geografia V(9), 5–68

Feio M (1981) O relevo do Sudoeste de Angola. Estudo de Geomorfologia', vol 67 (Segunda Série), Memórias da Junta de Investigações Científicas do Ultramar, p 326

Feria M, Martín-Banda R, Francés A, García-Lobón J, Mochales T, Rey-Moral C, Gumiel J, Escuder-Viruete J, Merino Martínez E, Oliveira A, Labaredas J, Marques E, Pereira E, Rodrigues J, Alves D (2021) Carta Geológica de Angola à escala 1:500 000, Carta de Síntese e Hidrogeológica de Angola e Memória Explicativa da folha 6 (2ª edição)'. UTE (IGME, LNEG, Impulso) - IGEO, Luanda, 194 pp

Foged N, Auken E, Christiansen AV, Sørensen KI (2013) Test site calibration and validation of airborne and ground-based TEM systems. Geophysics 78(2):E95–E106. https://doi.org/10.1190/geo2012-0244.1

Gärtner A, Houben GJ, Sitnikova MA, Miller RM, Wang F, Zieger-Hofmann M, Zieger J, Linnemann U (2023) Multiproxy sediment provenance analysis of two megafans in the Owambo Basin, Northern Namibia. J Geol Soc 180(2). https://doi.org/10.1144/jgs2022-065

Gomes CSF (1972) Subsídios para o conhecimento dos sedimentos subsuperficiais do Kalahari do sul de Angola (região da Môngua)',

Technical report, República Portuguesa, Estado de Angola, Direcção Provincial dos Serviços de Geologia e Minas, Luanda
Gumiel J, Martín-Banda R, Iglesias-Martínez M, Goicoechea P (2018) Carta Geológica de Angola à escala 1:250 000, folha Sul E-33/DJ (Ondjiva) e Memória Explicativa (2a edição)'. UTE (IGME, LNEG, Impulso) - IGEO, Luanda, 203 pp
Haddon IG (2005) The Sub-Kalahari Geology and Tectonic Evolution of the Kalahari Basin, South Africa', Ph.D. thesis, University of Witwatersrand, Johannesburg, South Africa
Hamutoko JT, Post VEA, Wanke H, Beyer M, Houben G, Mapani B (2019) The role of local perched aquifers in regional groundwater recharge in semi-arid environments: Evidence from the Cuvelai-Etosha Basin, Namibia. Hydrogeol J 27(7):2399–2413. https://doi.org/10.1007/s10040-019-02008-w
Himmelsbach T, Beyer M, Wallner M, Grünberg I, Houben G, Revermann R, Krewenka K, Schmiedel U, Olwoch J, Helmschrot J, Jürgens (2018) Deep, semi-fossil aquifers in Southern Africa: A synthesis of hydrogeological investigations in Northern Namibia in: Climate change and adaptive land management in Southern Africa - assessments, changes, challenges, and solutions. Biodivers Ecol 6:66–74. https://doi.org/10.7809/b-e.00306
Houben GJ, Kaufhold S, Miller RM, Lohe C, Hinderer M, Noll M, Hornung J, Joseph R, Gerdes A, Sitnikova M, Quinger M (2020) Stacked megafans of the Kalahari Basin as archives of paleogeography, river capture, and Cenozoic paleoclimate of southwestern Africa. J Sediment Res 90(9):980–1010. https://doi.org/10.2110/jsr.2020.46
INE (2016) Censo 2014 - Resultados definitivos do recenseamento geral da população e da habitação de Angola', Technical report 192 p. + annexes, Instituto Nacional de Estatística, Governo de Angola
Kirkegaard C, Auken E (2014) A parallel, scalable and memory efficient in-version code for very large-scale airborne EM surveys. Geophys Prospect 63(2):495–507. https://doi.org/10.1111/1365-2478.12200
Labaredas J, Oliveira A (2021a) Carta Geológica de Angola à escala 1:250 000, folha Sul E-34/G (Cuangar) e Memória Explicativa (2ª edição)'. UTE (IGME, LNEG, Impulso) - IGEO, Luanda, 121 pp
Labaredas J, Oliveira A (2021b) Carta Geológica de Angola à escala 1:250 000, folha Sul E-34/C (Luengue) e Memória Explicativa (2ª edição)'. UTE (IGME, LNEG, Impulso) - IGEO, Luanda, 140 pp
Labaredas J, Oliveira A (2021c) Carta Geológica de Angola à escala 1:250 000, folha Sul E-34/I (Dirico) e Memória Explicativa (2ª edição)'. UTE (IGME, LNEG, Impulso) - IGEO, Luanda, 114 pp
Legchenko A, Baltassat JM, Bobachev A, Martin C, Robain H, Vouillamoz JM (2004) Magnetic resonance sounding applied to aquifer characterization. Ground Water 42(3):363–373
Lindenmaier F, Miller R, Fenner J, Christelis G, Dill HG, Himmelsbach T, Kaufhold S, Lohe C, Quinger M, Schildknecht F, Symons G, Walzer A, van Wyk B (2014) Structure and genesis of the Cubango Megafan in Northern Namibia: implications for its hydrogeology. Hydrogeol J 22(6):1307–1328. https://doi.org/10.1007/s10040-014-1141-1
Lindenmaier F, Christelis G (2011) Groundwater for the North of Namibia: Summary Report of Activities of Phase I - Exploration of Ohangwena II Aquifer and Preliminary Isotope Study. Technical Report Vol. Ia of Technical Cooperation Project Groundwater for the North of Namibia, Tech. report, Department of Water Affairs and Forestry (DWAF), Namibia & Federal Institute for Geosciences and Natural Resources (BGR), Hannover, Germany
Lindenmaier F, Dill H, Dohrmann R, Fenner J, Gersdorf U, Kaufhold S, Kringel R, Ludwig R, Miller R, Nick A, Noell U, Walzer A (2012) Results of Analysis from Drill Holes on the Cubango Megafan. - Technical report C prepared for the Kalahari Research Project Development and Dating of Duricrusts as Base for a Paleogeographic and Hydrogeological Model of the Cuvelai-Etosha Basin in North Namibia, Tech. report, Hannover, Germany
Lubczynski MW, Roy J (2003) Hydrogeological interpretation and potential of the new magnetic resonance sounding (MRS) method. J Hydrol 283(1–4):19–40
Lubczynski MW, Roy J (2004) Magnetic resonance sounding: new method for ground water assessment. Ground Water 42(2):291–309
Lubczynski MW, Roy J (2007) Use of MRS for hydrogeological system parameterization and modeling. Bol Geol Min 118(3):509–530
Margane A, Bäumle R, Schildknecht F, Wierenga A (2005) Groundwater Investigations in the Oshivelo Region - Main Hydrogeological Report, Technical report 2001.2475.0 Volume IV.GW.1.1, Federal Ministry for Economic Cooperation and Development (Bundesministerium für Wirtschaftliche Zusammenarbeit und Entwicklung, BMZ)
Martín-Banda R, Gumiel J, Iglesias-Martínez M (2020) Carta Geológica de Angola à escala 1:250 000, folha Sul E-33/EK (Nehone-Cafima) e Memória Explicativa (2a edição)'. UTE (IGME, LNEG, Impulso) - IGEO, Luanda, 190 pp
Mendelsohn J, Mendelsohn S (2018) South West Angola - a portrait of land and life, Arte e Ciência
Miller RM, Pickford M, Senut B (2010) The geology, paleontology and evolution of the Etosha pan, Namibia: Implications for terminal for Kalahari deposition. S Afr J Geol 113(3):307–334. https://doi.org/10.2113/gssajg.113.3.307
Miller R (1992) The Etjo and Kalahari sediments of the Owambo Basin, Abstracts volume, Kalahari Symposium, November 7992, 42–51
Miller R (2008) The geology of Namibia, vol. 3. Ministry of Mines and Energy, Geological Survey, Windhoek
Monteiro Santos FA (2004) 1-D laterally constrained inversion of EM34 profiling data. J Appl Geophys 56:123–134
Motta Marques J (1967) Notícia sobre a província hidrogeológica de Pereira d'Eça. Boletim Dos Serviços De Geologia e Minas De Angola 16:31–40
Nascimento U, Farinha JAR (1967) Prospecção geofísica da possança das formações detríticas nas áreas dos concelhos de Roçadas e Cuanhama (Baixo Cunene) - Relatório Complementar, Tech. report 41, Serviço de Geotecnia, Divisão de Prospecção do LNEC
Nascimento U, Moura Esteves J, Farinha JAR (1966) Prospecção geofísica da possança das formações detríticas nas áreas dos concelhos de Roçadas e Cuanhama (Baixo Cunene), Tech. report 38, Serviço de Geotecnia, Divisão de Prospecção do LNEC
Nascimento U, Moura Esteves J, Farinha JAR (1967) Prospecção geofísica da possança das formações detríticas nas áreas dos concelhos de Roçadas e Cuanhama (Baixo Cunene) - Anexo, Tech. report 38, Serviço de Geotecnia, Divisão de Prospecção do LNEC
Neves Ferrão C (1961) A hidrogeologia e o problema do abastecimento de água ao Baixo Cunene (Angola). Garcia De Orta: Revista Da Junta De Investigaçoes Do Ultramar 9:515–538
Neves Ferrão CAC (1966) Utilização dos métodos geofísicos na prospecção de águas subterrâneas em regioes áridas e semiáridas. Boletim Dos Serviços De Geologia e Minas De Angola 13:5–12
Oliveira A, Sousa JC (2021) Carta Geológica de Angola à escala 1:250 000, folha Sul D-33/U - Chibemba e Memória Explicativa (2ª edição)'. UTE (IGME, LNEG, Impulso) - IGEO, Luanda, pp 206
Pacheco A (1976) Subsídio para o conhecimento do Sistema do Kalahari em Angola. Boletim Dos Serviços De Geologia e Minas 1:29–38

Ramalho EC, Francés AP, Martín-Banda R, Mateus T, Llorente JM, Famorosa A, Cuervo I, Lobón JL, Victorino AM (2023a) Contribuição de sondagens mecânicas e diagrafias para o estudo dos sistemas aquíferos multicamada transfronteiriços da bacia do Kalahari, Cunene, Angola', *in* 'XI Congresso Nacional de Geologia', pp 461–462

Ramalho EC, Francés AP, Santos FM, Victorino AdM (2023b) 3D electrical structure definition of aquifer systems in the Kalahari basin in Southern Angola based on legacy data reprocessing. J Appl Geophys 211. https://doi.org/10.1016/j.jappgeo.2023.104968

Represas P, Machadinho A, Alves D, Carvalho J, Borges J, Caldeira B (2021) Geologia do Subsolo in "Carta Geológica de Angola à escala 1:500 000, Carta de Síntese e Hidrogeológica de Angola e Memória Explicativa da folha 2 (1a edição), coord. of Pereira, E. and Ferreira, E. and Merino Martínez, E. and Rodrigues, J.F

Rodrigues JF, Marques E (2021) Geomorfologia in Carta Geológica de Angola à escala 1:500 000, Carta de Síntese e Hidrogeológica de Angola e Memória Explicativa da folha 5 (1a edição), coord. of Ferreira E, Merino-Martinez E, Pereira E, Rodrigues JF

Schildknecht F (2012) Groundwater exploration with TEM soundings in the Cuvelai-Etosha Basin. Report Part C - Groundwater for the North of Namibia (Cuvelai-Etosha Basin)', Technical report, Bundesanstalt Geowissenschaften und Rohstoffe, Hanover, Germany

Serrat-Capdevila A, Limones N, Marzo-Artigas J, Marcus W, Petrucci B (2022) Water Security and Drought Resilience in the South of Angola', World Bank. https://elibrary.worldbank.org/doi/abs/10.1596/37189

Sharma PV (1997) Environmental and engineering geophysics. Cambridge University Press

Sousa JC, Oliveira A, Máximo J (2021a) Carta Geológica de Angola à escala 1:250 000, folha Sul D-33/Q (Jamba) e Memória Explicativa (2ª edição)'. UTE (IGME, LNEG, Impulso) - IGEO, Luanda, pp 257

Sousa JC, Oliveira A, Máximo J (2021b) Carta Geológica de Angola à escala 1:250 000, folha Sul D-33/V (Cuvelai) e Memória Explicativa (2ª edição)'. UTE (IGME, LNEG, Impulso) - IGEO, Luanda, pp 211

Telford W, Geldart LP, Sheriff RE (1990) Applied Geophysics, 2nd edn, Cambridge University Press

Tikhonov N, Arsenin VY (1977) Solution of Ill-posed problems. Wiley, New York

Vouillamoz JM, Baltassat JM, Girard JF, Plata JL, Legchenko A (2007) Hydrogeological experience in the use of MRS. Bol Geol Min 118(3):531–550

Wallner M, Houben G, Lohe C, Quinger M, Himmelsbach T (2017) Inverse modeling and uncertainty analysis of potential groundwater recharge to the confined semi-fossil Ohangwena II Aquifer, Namibia. Hydrogeol J 25(8):2303–2321. https://doi.org/10.1007/s10040-017-1615-z